An Investigation of Gluon Density Parameters in $D^{*\pm}$ Meson Production

by Thomas Chapman

Magdalen College, Oxford University, OX1 4AU, England

DESY Summer Student Program 2007

Supervisor: **Hannes Jung**

Abstract

Inclusive production of $D^{*\pm}$ mesons in deep inelastic scattering with the H1 detector at HERA is studied. Values of photon virtuality of $5 < Q^2 < 100$ GeV^2 and scattering inelasticity $0.05 < y < 0.6$ are covered. In addition, the production of dijets with $D^{*\pm}$ mesons is analysed, with photon virtuality of $2 \leq Q^2 \leq 100$ GeV^2 and scattering inelasticity $0.05 \leq y \leq 0.7$. Single and double differential cross-sections are compared to predictions from the simulation program CASACDE. The normalisation and low-x power constants of the parton density function are varied in order to minimise the value of the statistical χ^2 test between data from the H1 detector and predictions from CASCADE.

1 Introduction

In order to produce Monte Carlo data to simulate specific processes, routines were written for hztool [3]. The results of these could then be compared to H1 data. A detailed description of the detector is given in [4].

1.1 QCD Modelling

In leading-order QCD calculations of deep inelastic *ep* scattering, heavy quarks are predominantly produced via the photon-gluon fusion process. In the dominant mechanism of charm anti-charm quark pair production a virtual photon interacts with a gluon, shown below in figure 1. This process is sensitive to the gluon density of the proton, and is therefore well suited to its investigation. Data collected both during 1999 and 2000 at HERA [1] and with the upgraded luminosity of HERA II during 2004 and 2006 are analysed [2].

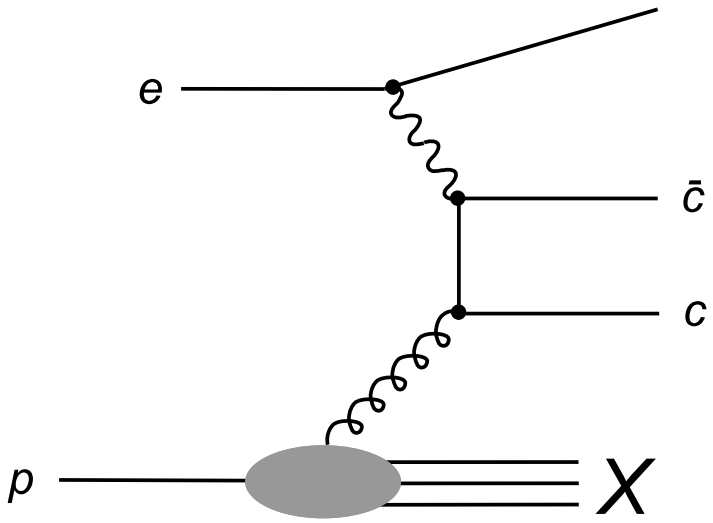

Figure 1: *Feynman Graph for charm production in the photon-gluon fusion process to leading order* α_s

The hadronization of gluons and quarks into jets theoretically displays a reduced sensitivity to fragmentation uncertainties while preserving sensitivity to the gluon density, thus more reliable theoretical predictions are expected. However, with regards to $D^{*\pm}$ meson production with accompanying dijets, currently only data taken prior to the upgrades to the luminosity of HERA were made are available [1], limiting the accuracy of calculation. However, it is still desirable for comparative purposes.

These processes are simulated using the Monte Carlo generator CASCADE, based upon Catani Ciafaloni Fiorani Marchesini (CCFM) evolution, using transverse momentum (k_T) factorised unintegrated parton distributions in the proton.

1.2 The Unintegrated Parton Density Function

In the 'naive proton model', the proton in ep scattering is approximated as being composed of non-interacting partons. The cross-section for a lepton electromagnetically scattering from a parton is then dependent on the parton density function, the probability density of finding a quark of given flavour and charge and carrying a fraction x (the Bjorken scaling variable) of the proton momentum, and leads to a structure function independent of Q^2 (the squared four-momentum of the exchanged boson). This method has been shown to be insufficient to account for behaviour at high energies, where processes such as pre-interaction gluon radiation from the quarks are significant.

The CCFM approach of CASCADE is an attempt to provide a description for the cross-section of the interaction that is valid for a broad range of x, covering low x, where the splitting of a gluon from the proton contributes strongly and can lead to a quark anti-quark pair (the subject of this study), and high x, where the parton density is approximately independent of the transverse momentum of the partons.

This cross-section is factorised into a scattering cross-section and a k_T-factorised unintegrated parton density function. The unintegrated parton density function is itself then treated as a convolution of a starting distribution and a perturbative evolution. The parameters of the starting distribution can be adjusted to minimise the value of χ^2 of the difference between theory, T, and data, D, where

$$\chi^2 = \sum_i \left(\frac{(T-D)^2}{\sigma_i^{2\ stat} + \sigma_i^{2\ uncorr}} \right) \tag{1}$$

For small x final state processes, the starting distribution of the parton density function can be approximated as proportional to

$$xg(x,\mu_0^2) \ \propto \ Nx^{-B_g} \tag{2}$$

and it is these parameters, N and B_g, that are altered in this study. A thorough discussion of these unintegrated parton density functions can be found in [5].

2 Routine Construction

Routines for hztool were modified to reproduce the data presented in both previous studies [1] and [2]. For the HERA II data, the routines were altered to implement kinematic variable cuts of $5 < Q^2 < 100$ GeV^2 and $0.05 < y < 0.6$. Further cuts on the transverse momentum of the $D^{*\pm}$ meson of $p_T(D^{*\pm}) > 1.5$ GeV and on the pseudorapidity of the $D^{*\pm}$ meson of $\mid \eta \mid < 1.5$ were imposed, both as measured in the laboratory frame. Gluon-density set J2003, subset 3 [7] was used for 920 GeV protons and 27.6 GeV electrons.

For the HERA data prior to upgrading, the hztool routine was again altered to implement kinematic variable cuts of $2 \leq Q^2 \leq 100$ GeV^2 and $0.05 \leq y \leq 0.7$. Further cuts on the transverse momentum of the $D^{*\pm}$ meson of $1.5 \leq p_T(D^{*\pm}) \leq 15$ GeV and on the pseudorapidity of the $D^{*\pm}$ meson of $\mid \eta \mid \leq 1.5$ were imposed, both as measured in the laboratory frame. Gluon-density set A0 [8] was used for 920 GeV protons and 27.5 GeV electrons.

Data were also produced with cuts placed on the transverse momentum of the $D^{*\pm}$ meson in the photon-proton centre-of-mass frame where $p_T^*(D^{*\pm}) > 2.0$ GeV.

For the '$D^{*\pm}$ meson with dijets' sample, all previous kinematic, momentum and pseudorapidity cuts in the lab frame were applied. It was further demanded that two or more jets were produced in an *ep* collision event. These jets were subsequently ordered by their transverse energy as measured in the Breit frame (or 'brick wall' frame), E_T^{Breit}. The two most energetic jets were required to have pseudorapidities as measured in the laboratory frame in the range -1 $\leq \eta_{lab} \leq$ 2.5. The jet with the highest E_T^{Breit}, the leading jet, was required to have $E_T^{Breit} \geq 4$ GeV, while the next most energetic jet was required to have $E_T^{Breit} \geq 3$ GeV. In addition to differential cross-section calculations of Q^2, x, p_T, etc..., plots were made of E_T^{Breit} of the most energetic jet and of M_{jj}, the invariant mass of the system of the jet containing the $D^{*\pm}$ meson and the jet with the highest E_T^{Breit} which did not contain the $D^{*\pm}$ meson. In order to determine the presence of the $D^{*\pm}$ meson within a jet, the four-vector of the reconstructed $D^{*\pm}$ meson was used rather than the four-vector of its three decay particles in the E-recombination scheme [6].

3 $D^{*\pm}$ Meson Cross Sections

All simulations were run with 5×10^6 events. For the HERA II data set [2], the CASCADE simulations produced results in excellent agreement with both experimental results and previous Monte Carlo studies. These results are displayed in figures 2 to 11.

For the HERA data set taken at luminosities prior to upgrading, the CASCADE simulations produced results in accordance with both experimental results and previous Monte Carlo studies for cases when cuts on Q^2, y, $D^{*\pm}$ momentum and pseudorapidity were applied, as well as for further cuts in the photon-proton centre of mass frame. These results are displayed in figures 12 and 13 and figures 14 and 15 respectively.

For the '$D^{*\pm}$ meson with dijets' sample, the CASCADE predictions were in close agreement with the data for differential cross-sections in Q^2, x and E_T^{Breit} of the most energetic jet. The CASCADE generator has a tendency to slightly over-estimate the cross-section in these situations, as can be seen in figures 16 to 18. However, for the differential cross-section as a function of the invariant mass of the dijet system M_{jj}, the CASCADE data produced in the 06-240 hztool routine deviated significantly from the data and from previous CASCADE studies, as seen is figure 19. The routine displays a skew in favour of higher values of M_{jj}. The reason for this is at present unknown.

4 Fitting

The hztool routines were implemented in the fitting version of CASCADE and scans of the parameters N and B_g were performed in order to narrow the range over which the fitting program would be run in order to minimise the long run-time of the fitting program. Using HERA II data [2], a scan of the constants N and B_g over the ranges $0.4 \leq N \leq 0.5$ and $0.025 \leq B_g \leq 0.030$ respectively using 10 divisions was performed and χ^2 calculated. The scan was run using 5×10^5 events over all single differential cross-sections and over all double-differential cross-sections, and χ^2 normalised to the number of degrees of freedom (52).

The scan, despite being a preliminary to fitting, produced results indicating an improvement in the agreement between CASCADE output and HERA II data over the stand-alone version of CASCADE for this process (using gluon-density set J2003, subset 3 [7]). A sample of the results of the scans of single and double differential cross-sections are shown in figures 20 and 21 respectively. Graphical plots of the values of χ^2 for N and B_g are shown in figures 22 and 23 respectively for single differential cross-sections and figures 24 and 25 for double differential cross-sections.

There is a clear minimum observed in both cases for the normalisation constant of the unintegrated parton density function. For the single differential cross-section, the value of N is around 0.465, and for the double differential cross-section it appears, as expected, to be of a similar value.

However, for B_g, there was no statistically significant variation in χ^2 in the range scanned for either single or double differential cross-sections. It is highly likely that the production of $D^{*\pm}$ mesons is not independent of B_g, but merely that a larger scan range would be needed to show this sensitivity. Further scanning was attempted in order to more precisely determine N and observe a minimum in B_g, but unfortunately due to an undetermined data transfer error the data was lost and insufficient time to reproduce it available.

The parameters N and B_g should, entering only into the parton density function of the starting distribution, be independent of the final state of the system. A preliminary study of a different system also using the CASCADE Monte Carlo generator was concurrently performed at DESY [9]. The results at this point in time indicate that the value of N is different in J/ψ production, but further study into this is required.

5 Summary

The hztool routines produced for CASCADE satisfactorily simulated the production of $D^{*\pm}$ mesons. The routine for the paper 06-240 [1] will need reviewing before integrating into the hztool manual in order to determine the origin of the difference in M_{jj}. However, the routine for the paper 07-072 [2] is ready for general use.

With regards to the fitting process, it is clear that the production of $D^{*\pm}$ mesons is sensitive to the normalisation of the unintegrated parton density function and that an optimum value exists. Further study of B_g is required. Other final state processes also require further investigation to determine from where the difference in N originates.

6 Acknowledgments

I would like to thank Dr. Hannes Jung for his continued supervision and generous support throughout this project. I would also like to thank Axel Cholewa and the rest of the H1 team for their help and time. Finally I would like to thank my summer-student colleagues Plamen Petrov and Federico von Samson-Himmelstjerna for their contributions to this project.

References

[1] H1 Collaboration, *Production of $D^{*\pm}$ Mesons with Dijets in Deep-Inelastic Scattering at HERA* (December 2006, DESY 06-240)

[2] H1 Collaboration, *$D^{*\pm}$ Meson Production in Deep-Inelastic Scattering at HERA* (July 19-25, 2007, Manchester, DESY 07-072)

[3] J. M. Butterworth, S. Butterworth, B. M. Waugh, W. J. Stirling and M. R. Whalley, [arXiv:hep-ph/0412139]. http://www.cedar.ac.uk, *hztool version 4.2*

[4] I. Abt *et al.* [H1 SPACAL Group Collaboration], Nucl. Instrum. Meth. **A 386** (1997) 310; I. Abt *et al.* [H1 SPACAL Group Collaboration], Nucl. Instrum. Meth. **A 386** (1997) 348

[5] Axel Cholewa, *Transverse Momentum of Gluons in ep-Scattering at HERA* (November 2006), ISSN 1435-8085

[6] k_T cluster algorithm 14 of the the hztool routine hzjtfind in CASCADE

[7] M. Hansson and H. Jung, *Status of CCFM: Un-integrated gluon densities*, hep-ph/0309009

[8] H. Jung, *Procs of the XII International Workshop on Deep Inelastic Scattering (DIS 2004)*, hep-ph/0411287

[9] Plamen Petrov, *Determination of Unitegrated Parton Density Functions in J/ψ Production at HERA* (Summer student report 2007)

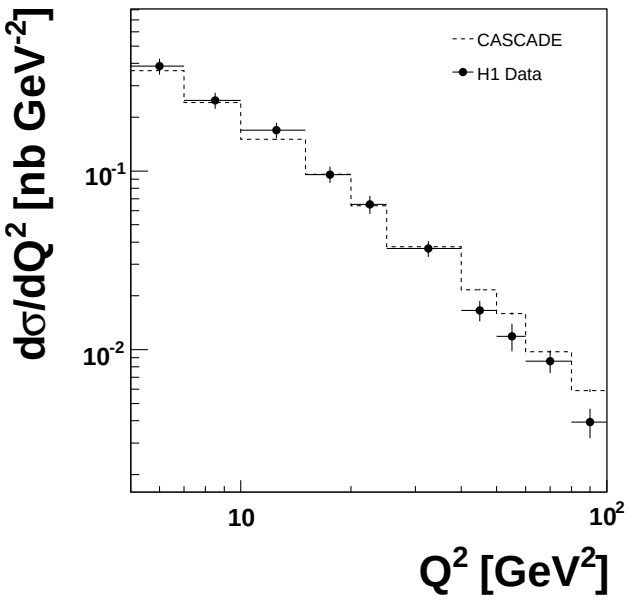

Figure 2: Differential cross-section as a function of Q^2 with kinematic cuts and parameters based upon paper 07-072 [2]

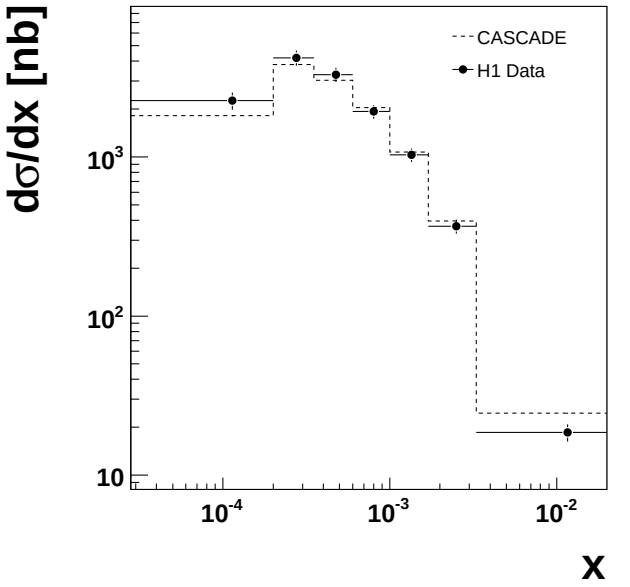

Figure 3: Differential cross-section as a function of x with kinematic cuts and parameters based upon paper 07-072 [2]

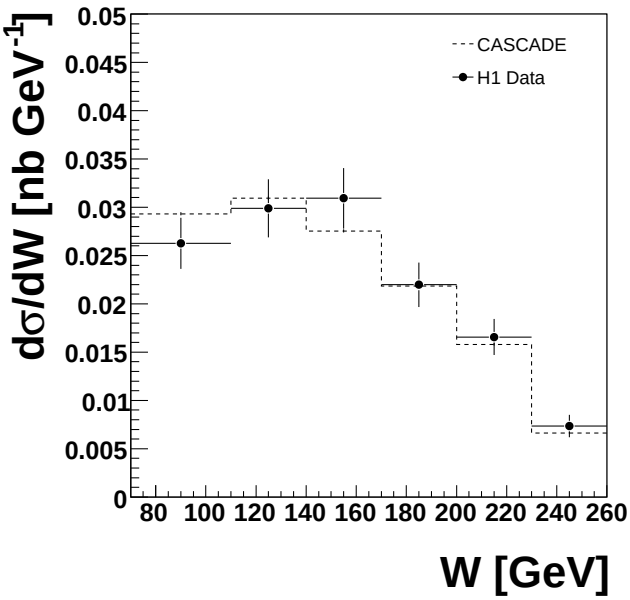

Figure 4: Differential cross-section as a function of W with kinematic cuts and parameters based upon paper 07-072 [2]

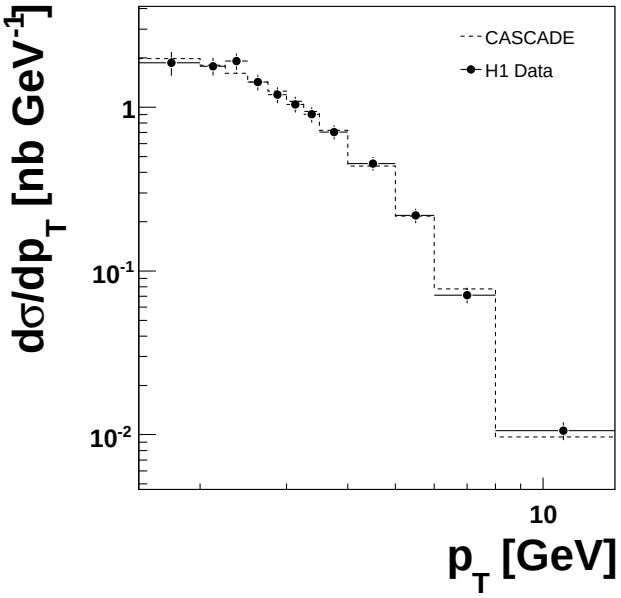

Figure 5: Differential cross-section as a function of p_T with kinematic cuts and parameters based upon paper 07-072 [2]

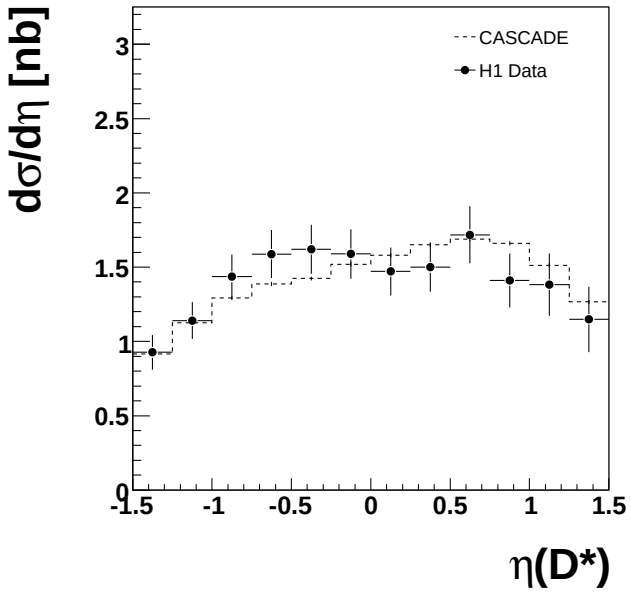

Figure 6: Differential cross-section as a function of $\eta(D^{*\pm})$ with kinematic cuts and parameters based upon paper 07-072 [2]

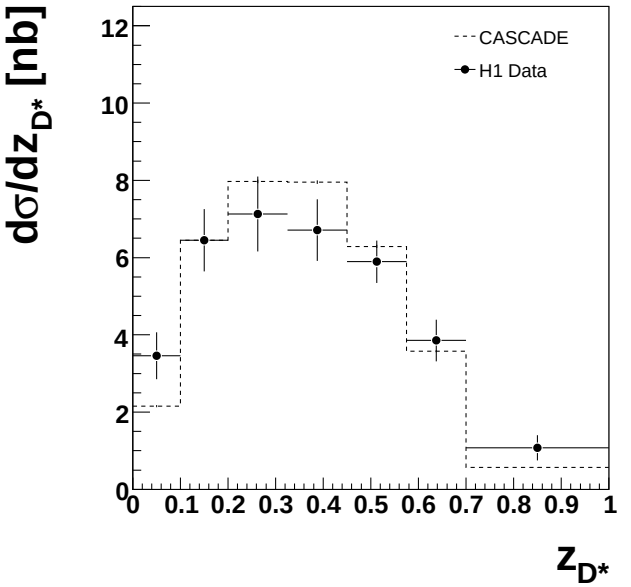

Figure 7: Differential cross-section as a function of $z_{D^{*\pm}}$ with kinematic cuts and parameters based upon paper 07-072 [2]

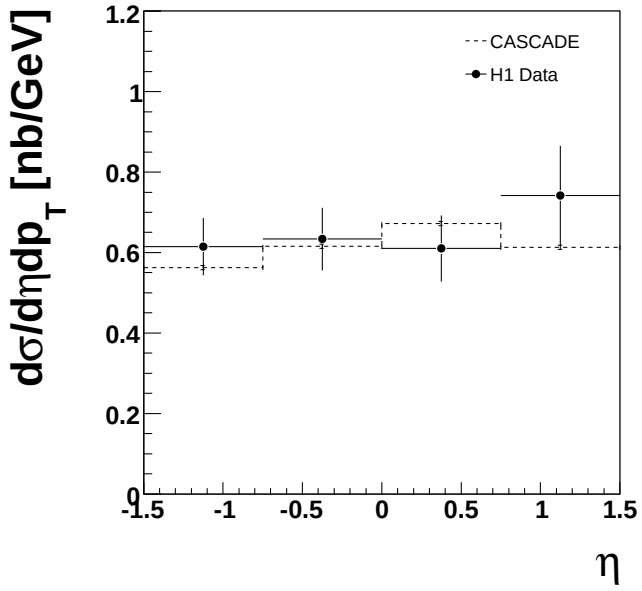

Figure 8: Double differential cross-section as a function of $\eta(D^{*\pm})$ and $1.5 < p_T < 2.5$ GeV with kinematic cuts and parameters based upon paper 07-072 [2]

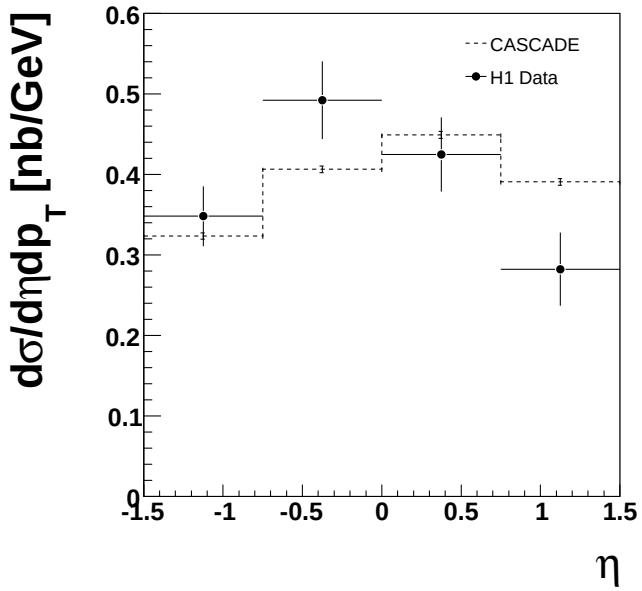

Figure 9: Double differential cross-section as a function of $\eta(D^{*\pm})$ and $2.5 < p_T < 3.5$ GeV with kinematic cuts and parameters based upon paper 07-072 [2]

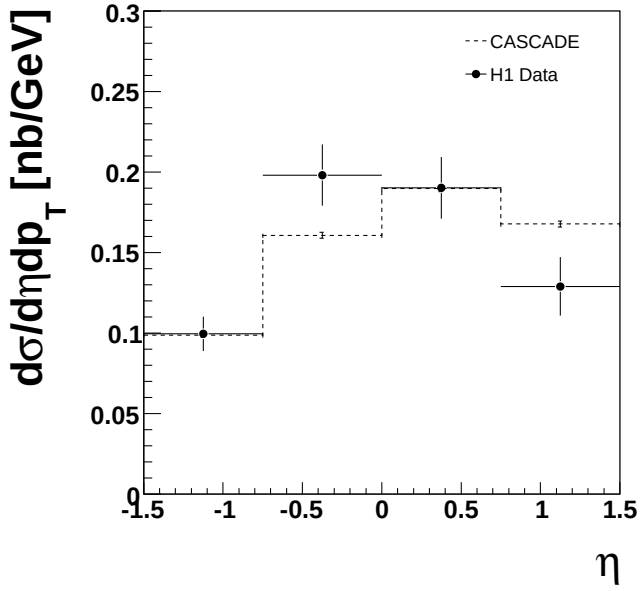

Figure 10: Double differential cross-section as a function of $\eta(D^{*\pm})$ and $3.5 < p_T < 5.5$ GeV with kinematic cuts and parameters based upon paper 07-072 [2]

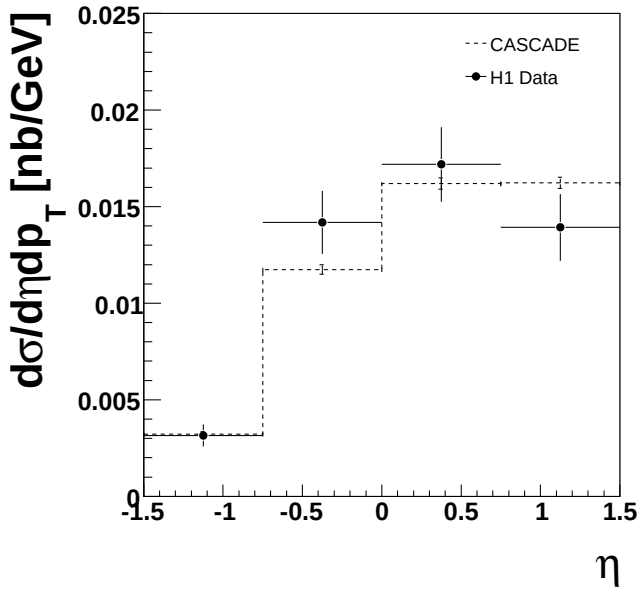

Figure 11: Double differential cross-section as a function of $\eta(D^{*\pm})$ and $5.5 < p_T < 14$ GeV with kinematic cuts and parameters based upon paper 07-072 [2]

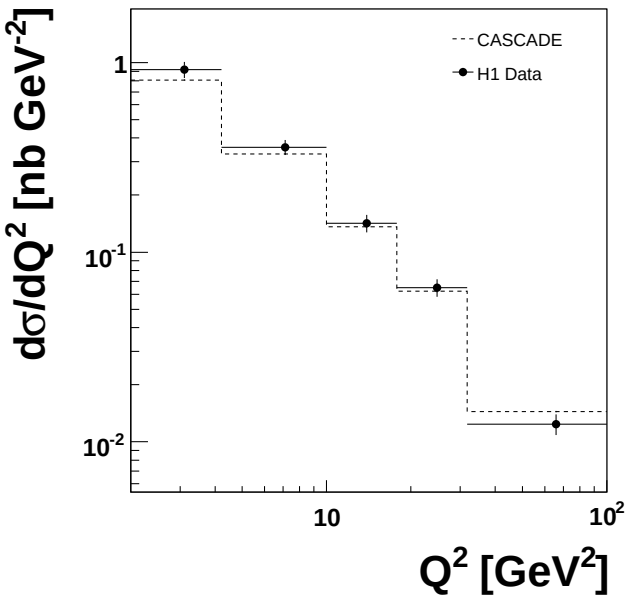

Figure 12: Differential cross-section as a function of Q^2 with kinematic cuts and parameters based upon paper 06-240 [1]

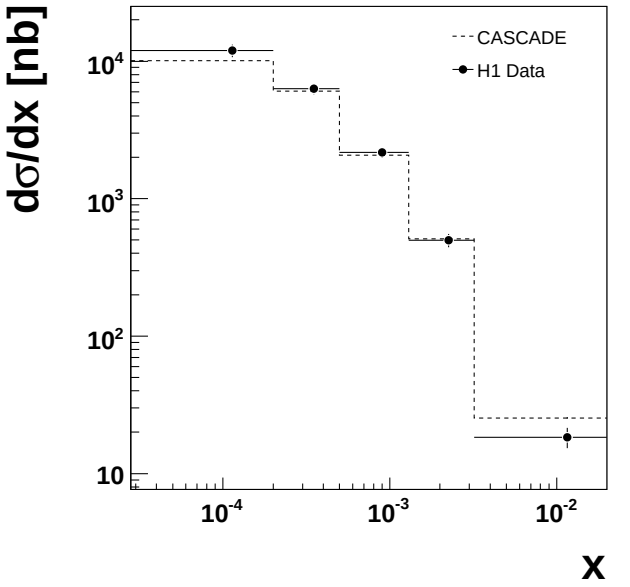

Figure 13: Differential cross-section as a function of x with kinematic cuts and parameters based upon paper 06-240 [1]

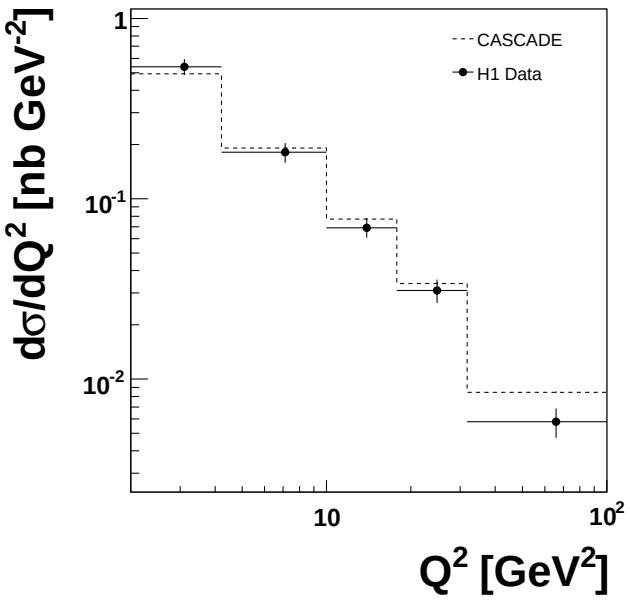

Figure 14: Differential cross-section as a function of Q^2 with further cuts in the photon-proton cms frame and parameters based upon paper 06-240 [1]

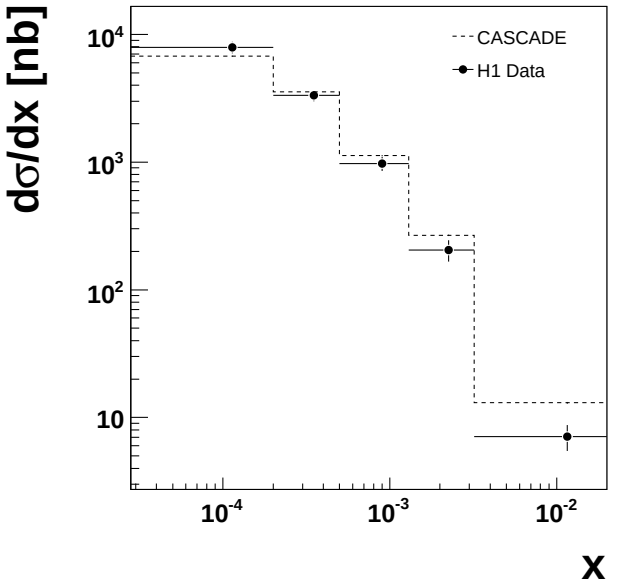

Figure 15: Differential cross-section as a function of x with further cuts in the photon-proton cms frame and parameters based upon paper 06-240 [1]

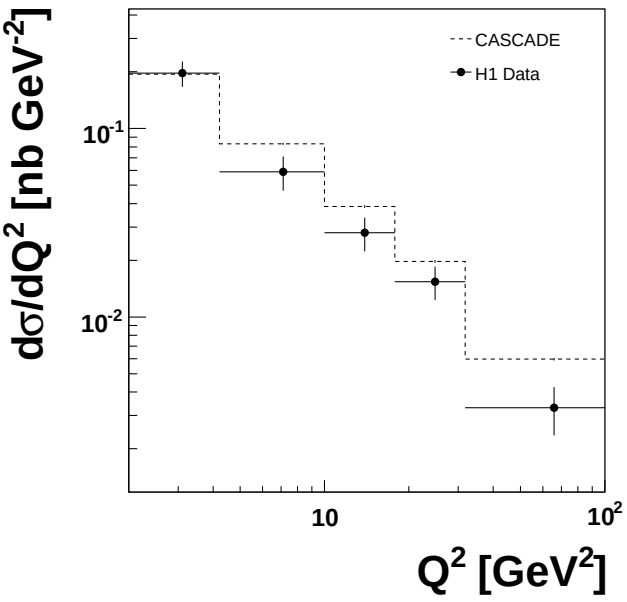

Figure 16: Differential cross-section as a function of Q^2 with further dijet cuts and parameters based upon paper 06-240 [1]

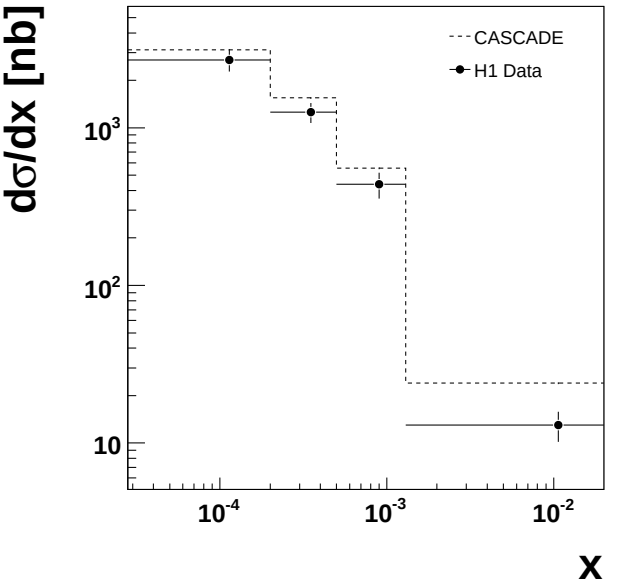

Figure 17: Differential cross-section as a function of x with further dijet cuts and parameters based upon paper 06-240 [1]

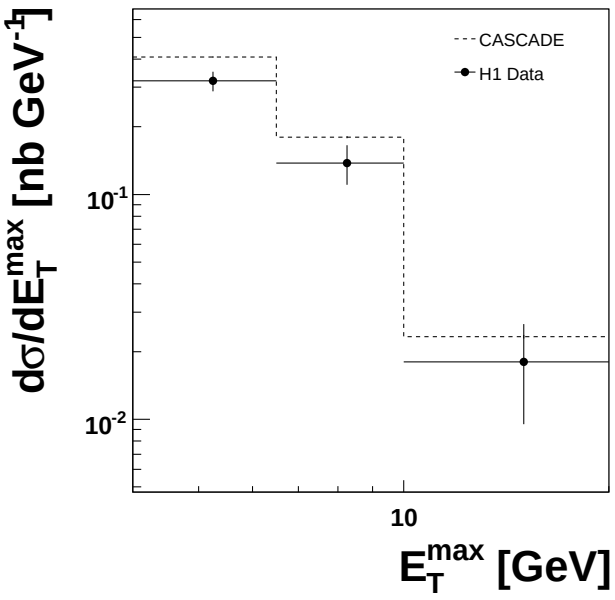

Figure 18: Differential cross-section as a function of the maximum of E_T^{Breit} with further dijet cuts and parameters based upon paper 06-240 [1]

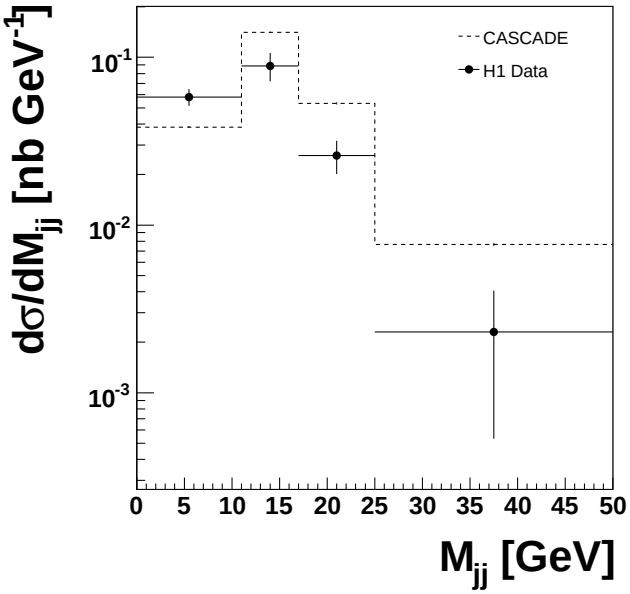

Figure 19: Differential cross-section as a function of M_{jj} with further dijet cuts and parameters based upon paper 06-240 [1]

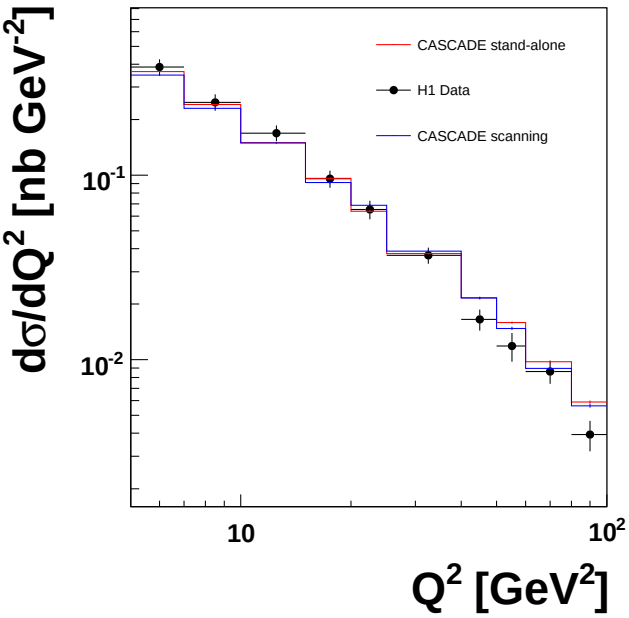

Figure 20: Stand-alone and scanning-mode CASCADE data with HERA II data for the differential cross-section of Q^2 based upon paper 07-072 [2]

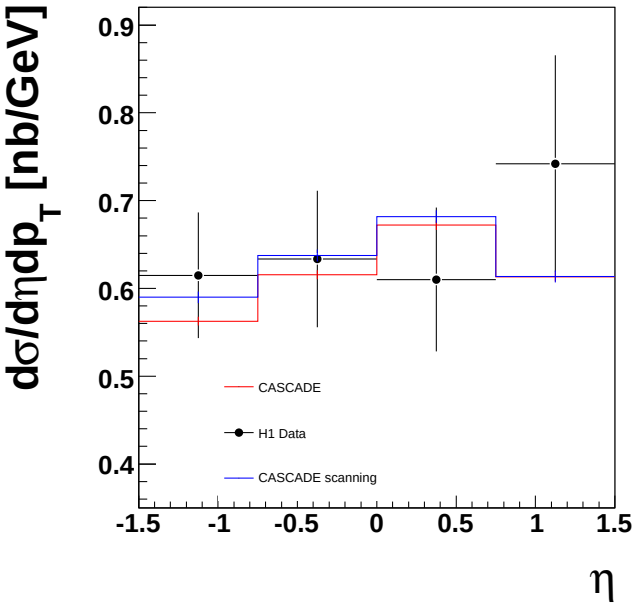

Figure 21: Stand-alone and scanning-mode CASCADE data with HERA II data for the second differential cross-section of $\eta(D^{*\pm})$ and $1.5 < p_T < 2.5$ GeV based upon paper 07-072 [2]

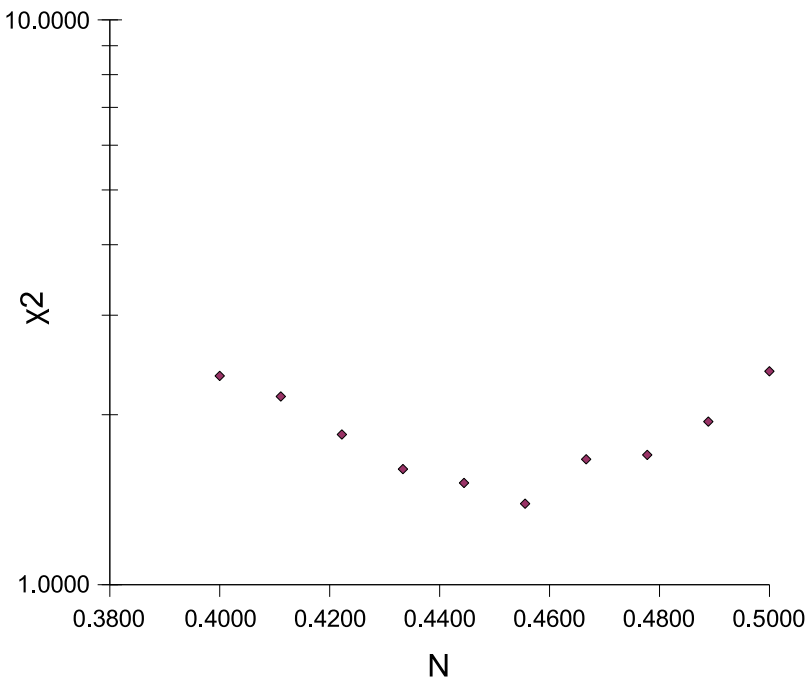

Figure 22: χ^2 plot of N using single differential cross-sections based upon paper 07-072 [2]

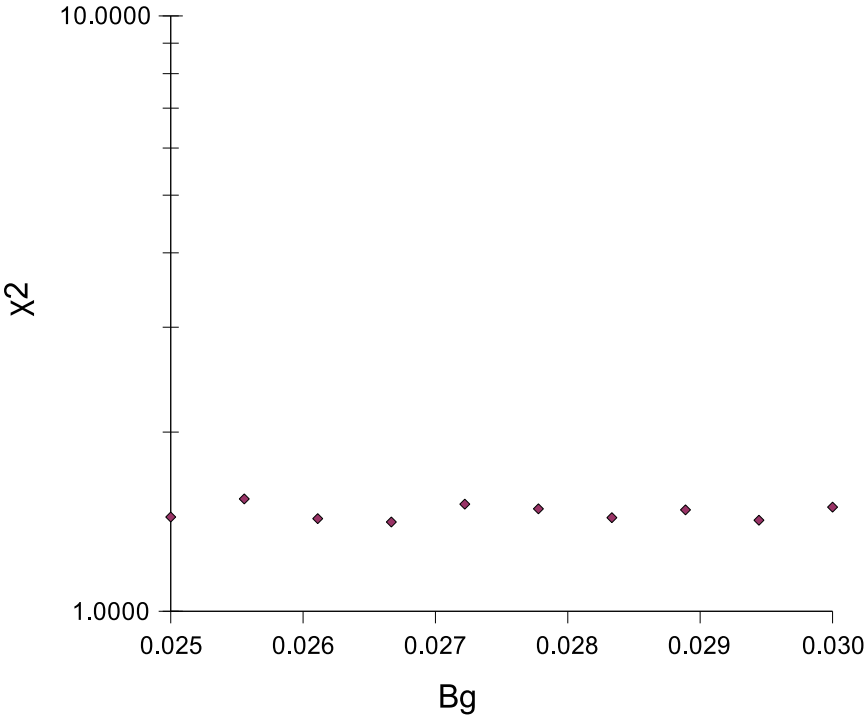

Figure 23: χ^2 plot of B_g using single differential cross-sections based upon paper 07-072 [2]

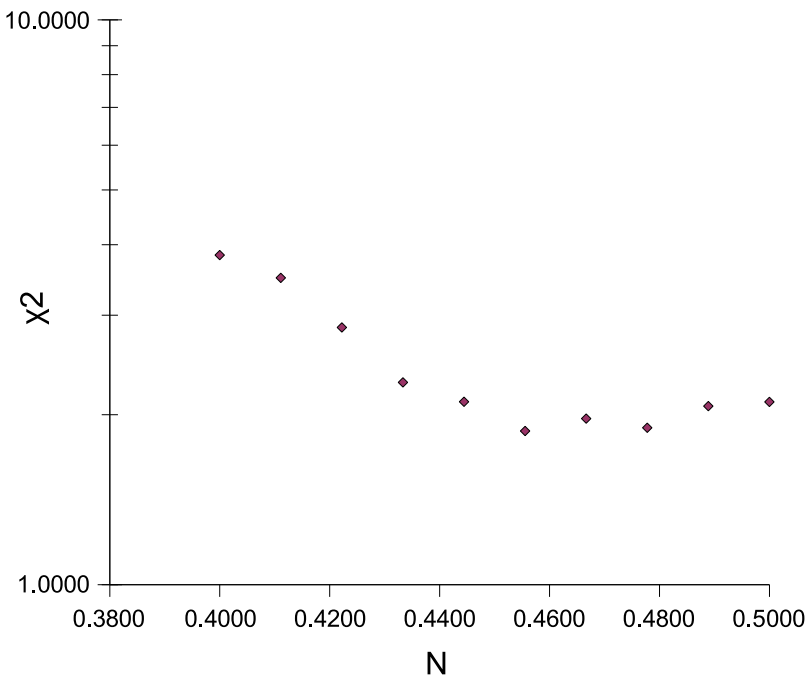

Figure 24: χ^2 plot of N using double differential cross-sections based upon paper 07-072 [2]

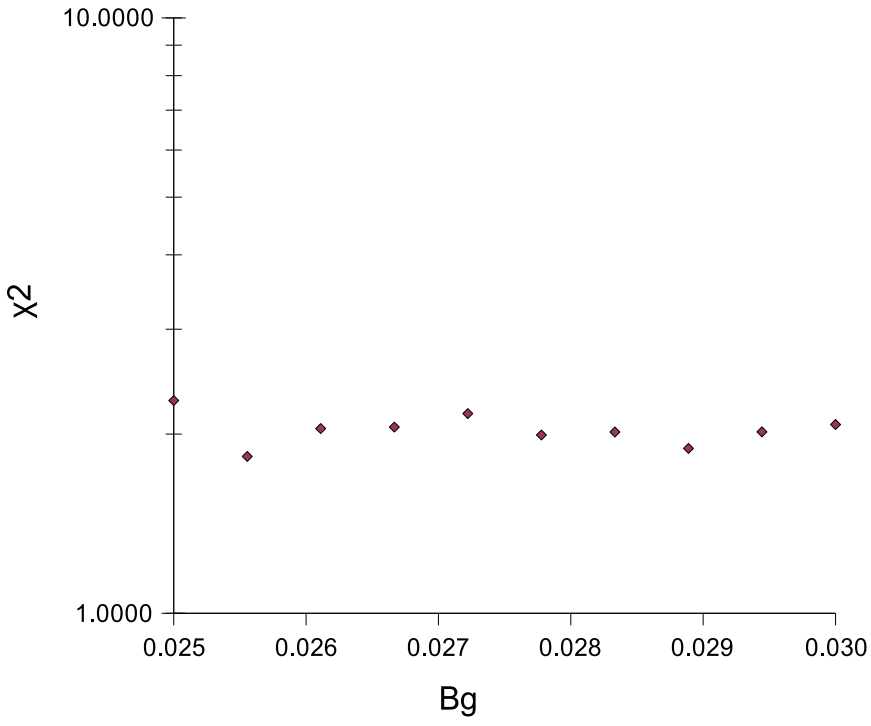

Figure 25: χ^2 plot of B_g using double differential cross-sections based upon paper 07-072 [2]